Published in final edited form as:

Environ Pollut. 2017 January ; 220(Pt A): 469–477. doi:10.1016/j.envpol.2016.09.089.

Colloidal properties and stability of aqueous suspensions of few-layer graphene: Importance of graphene concentration

Yu Su[a], **Guoqing Yang**[a], **Kun Lu**[a], **Elijah J. Petersen**[b], and **Liang Mao**[a,*]

[a]State Key Laboratory of Pollution Control and Resource Reuse, School of the Environment, Nanjing University, Nanjing 210093, P. R. China

[b]Material Measurement Laboratory, Biosystems and Biomaterials Division, National Institute of Standards and Technology, 100 Bureau Drive, Stop 8311, Gaithersburg, MD 20899-0001, USA

Abstract

Understanding the colloidal stability of graphene is essential for predicting its transport and ecological risks in aquatic environments. We investigated the agglomeration of ^{14}C-labeled few-layer graphene (FLG) at concentrations spanning nearly four orders of magnitude (2 μg/L to 10 mg/L) using dynamic light scattering and sedimentation measurements. FLG agglomerates formed rapidly in deionized water at concentrations > 3 mg/L. From 1 mg/L to 3 mg/L, salt-induced agglomeration was decreased with dilution of FLG suspensions; the critical coagulation concentration of the more concentrated suspension (3 mg/L) was significantly lower than the dilute suspension (1 mg/L) in the presence of NaCl (1.6 mmol/L and 10 mmol/L, respectively). In contrast, FLG underwent slow agglomeration and settling at concentrations ≤ 0.1 mg/L in NaCl solutions and ambient waters with low ionic strength (< 10 mmol/L). Although salt-induced agglomeration led to 67 % reduction in number of small FLG (25 nm to 50 nm) according to atomic force microscopy characterization, transition from concentrated to dilute suspension retarded the removal of the small FLG. Additionally, the small FLG exhibited greater bioaccumulation in zebrafish embryo and stronger chorion penetration ability than larger ones. These findings suggest that FLG at more environmentally relevant concentration is relatively stable and may have implications for exposure of small FLG to ecological receptors.

Keywords

graphene; nanomaterial; agglomeration; sedimentation; bioaccumulation

1. Introduction

Graphene, a new carbon-based nanomaterial (CNM), since first isolated by Novoselov et al. in 2004 (Novoselov et al., 2004), has attracted increasing attention because of its extraordinary properties and potential applications (Geim, 2009; Novoselov et al., 2012), such as in composites (Ramanathan et al., 2008; Stankovich et al., 2006), ultrasensitive sensors (Schedin et al., 2007), and transparent conductive films (Eda et al., 2008; Wang et

*Corresponding author. Tel: +86 025-83594532. lmao@nju.edu.cn (Liang Mao).

al., 2008). Currently, graphene is being incorporated into a broad range of commercial products at a rapid rate (Segal, 2009). The increasing production and use of graphene will inevitably lead to its release into the environment. Unfortunately, the environmental behaviors of graphene are still largely unknown. To date, the majority of studies have focused on the human health-related issues of graphene (Bussy et al., 2013; Duch et al., 2011; Schinwald et al., 2012; Seabra et al., 2014; Yang et al., 2011; Yang et al., 2010; Zhang et al., 2010), with only a limited number of studies on potential ecological risks (Guo et al., 2013; Hu et al., 2014; Hu et al., 2015). The exposure of nanomaterials is directly determined by their transport and fate in the environment (Batley et al., 2012; Lowry et al., 2012; Maurer-Jones et al., 2013). Once released into aquatic systems, graphene is likely to interact with ubiquitous inorganic ions and natural organic matter (NOM). Changes in graphene size and shape resulting from agglomeration may subsequently alter its mobility as well as its reactivity and toxicity (e.g., to algal cells and wheat roots) (Hu et al., 2014; Hu et al., 2015). Therefore, knowledge of the agglomeration behavior of graphene in aquatic environments is essential for predicting its fate and potential for ecological exposure.

Agglomeration and stability of fullerene (nC_{60}) (Anderson and Barron, 2005; Bouchard et al., 2009; Chen and Elimelech, 2006, 2008, 2009), carbon nanotube (CNT) (Sano et al., 2001; Smith et al., 2008; Smith et al., 2009), and graphene oxide (GO) (Chowdhury et al., 2013; Chowdhury et al., 2015; Huang et al., 2016; Konkena and Vasudevan, 2012; Wu et al., 2013) have been extensively studied in the literature. These studies showed that the agglomeration of CNMs follows the Derjaguin-Landau-Verwey-Overbeek (DLVO) theory, and the CNM-specific properties have strong effects on the colloidal stability of CNMs. For example, the critical coagulation concentration (CCC) of cations was found to increase with the increasing surface oxygen contents of CNT and GO (Chowdhury et al., 2015; Smith et al., 2009; Yi and Chen, 2011). This suggests that pristine graphene with a hydrophobic lattice may undergo layer-to-layer agglomeration in water at low ionic strength (IS). As mass concentration affects particle number and the rate of collisions between colloids that have small Hamaker constants and low surface potentials (Hsu and Liu, 1998), salt-induced agglomeration is expected to be reduced at a low graphene concentration. However, no study has yet been conducted to quantitatively establish the agglomeration kinetics of graphene as a function of electrolyte concentration or to test the impact of mass concentration on its colloidal stability. In addition, for graphene with nonuniform particle size distribution, agglomeration and settling cause increased heterogeneity in water column (Petersen et al., 2015). It is likely that small graphene particles remain suspended for longer time periods in dilute suspensions than the thicker ones. Characterization of size distribution of the suspended CNMs is over-looked by the previous investigations. Moreover, it is very important to evaluate the environmental risks of small graphene when ecological receptors tend to ingest small nanomaterials (Mu et al., 2012; Silva et al., 2014; Zhao and Wang, 2012).

The objective of this paper is to ascertain the impact of mass concentration on agglomeration and stability of ^{14}C-labeled graphene, which mainly comprised four graphene layers (Guo et al., 2013) and were defined as few-layer graphene (FLG) in our previous work (Feng et al., 2015; Lu et al., 2015; Mao et al., 2016). The potential ecological risks of the suspended small FLG (S-FLG) were also investigated. The agglomeration kinetics of FLG (0.1 mg/L to

10 mg/L) at varying IS were investigated by using dynamic light scattering (DLS) method. To investigate the state of agglomeration of FLG at concentrations (2 μg/L to 107 μg/L) that are below the detection limit of DLS and most other analytical techniques, sedimentation kinetics in simple electrolyte solutions and ambient water samples were performed via radioactivity measurements. While performing experiments with varying compositions is necessary to yield a mechanistic understanding, it is critical to verify that those trends are still observed in water samples from the natural and engineered environment because some factors such as the type of NOM vary widely among water sources and the NOM composition can impact the fate of environmental pollutants such as nanomaterials (Akkanen et al., 2001; Pakarinen et al., 2013). After the size distribution of suspended FLG during the settling experiments was characterized by atomic force microscopy (AFM), we preparaed S-FLG by prolonged sonication and evaluated if biological uptake of FLG by zebrafish (*Denio rerio*) embryo is size-dependent.

2. Materials and methods

2.1. Graphene synthesis and characterization

Synthesis of 14-labeled FLG by graphitization and exfoliation of sandwich-like $FePO_4$/dodecylamine hybrid nanosheets has been described in our previous study (Guo et al., 2013). Using X-ray photoelectron spectroscopy (XPS), the atomic ratio of C:O in the FLG was determined to be 89:6 (the remaining 5 % is 1.4 % of H and 3.6 % of N) (Guo et al., 2013), and carbonyl (C=O), hydroxyl (C-OH), and carboxyl (COOH) functional groups were found on the FLG surface (Feng et al., 2015). Notably, the oxygen was introduced by the addition of ^{14}C-phenol during the FLG synthesis, not by oxidation. The specific radioactivity of FLG was determined to be (16.0 ± 0.6) mCi/g (n=3; uncertainties always indicate standard deviation values if not specified). A stock suspension of FLG (20 mg/L) was prepared following the procedures that are provided in the Supporting Information (SI), and its radioactivity was determined via liquid scintillation counting (LSC) (LS 6500, Beckman Coulter).

2.2. Electrophoretic mobility measurements

The electrophoretic mobility (EPM) of FLG (1 mg/L to 10 mg/L) was measured at varying NaCl and NOM concentration at pH 7.0 and 25 °C using a disposable folded capillary cell (Nano ZS, Malvern). Because the calculation of zeta potential values from EPM measurements uses the Henry equation and the Smoluchowski approximation which assumes spherical particles, it is problematic to use this approach for non-spherical CNMs (Petersen and Henry, 2012); EPM values are reported instead. As described in the SI, Suwannee River NOM (SRNOM) (RO isolation, International Humic Substances Society) was used as a model NOM and a stock solution of SRNOM was prepared, which had a total organic carbon (TOC) content of (8.6 ± 0.1) mg/L (n=3). The background TOC content in the DI water was around 0.3 mg/L. For each solution condition, six measurements were conducted for each of three samples.

2.3. Graphene agglomeration and sedimentation kinetics

DLS (Nano ZS, Malvern) was used to measure the intensity-averaged hydrodynamic diameter (D_h) of FLG as functions of time and NaCl concentration in the absence and presence of SRNOM. For each agglomeration experiment, equal volumes (0.5 mL) of the diluted FLG stock suspension and NaCl solution in the absence and presence of SRNOM were separately pipetted into a disposable polystyrene cuvette to yield a specific FLG, electrolyte and/or SRNOM concentration. The capped cuvette was then briefly vortexed, placed in the DLS instrument, and the measurements were started immediately. The scattered light intensity was detected by a photodetector at a scattering angle of 90°, the D_h was recorded every 10 s by autocorrelation function until D_h reached 1.5-fold of the initial D_h or until 360 data points had been acquired (Chowdhury et al., 2013; Smith et al., 2008). All agglomeration experiments were conducted in triplicate at pH 7.0, at which the FLG is stable at low IS. Detailed equations and parameters for calculation attachment efficiency (α_a) and CCC values are provided in the SI. The FLG concentration in the DLS measurements was quantified by radioactivity measurements and ranged from 0.1 mg/L to 10 mg/L. However, FLG concentrations below 1 mg/L did not provide a sufficient signal for accurate DLS measurements and were not included in further analysis.

The long-term stability of FLG at low concentrations (2 μg/L to 107 μg/L) were evaluated both in well-controlled simple electrolyte solution and in natural or engineered aqueous systems. Eight ambient waters were collected and characterized. Details for water sampling locations and water analysis are provided in Table S1 and the SI. The sedimentation experiments were initiated by mixing 25 mL of NaCl solution (0 mmol/L to 500 mmol/L, pH=7.0) or each of the eight waters with the FLG stock suspension in 40 mL amber glass vials (95 mm by 27.5 mm, CNW Technologies) with Teflon-lined screw caps. The mixture was then vortexed for 10 s and was left undisturbed for up to 28 d at 25 °C. The concentrations of suspended FLG in different treatments were monitored via radioactivity measurements (detailed procedures are provided in the SI). Preliminary experiments showed that the total volume of the mixture (1 mL to 40 mL) had insignificant influence on the sedimentation of FLG (Fig. S1). Control measurements performed by adding the ^{14}C-labeled FLG to each of the water samples, mixing them, and then immediately sampling the radioactivity using LSC did not indicate a statistically significant matrix interference for any of the waters. All settling experiments were conducted in triplicate to verify experimental reproducibility. To determine the particle size of the suspended FLG, identical sedimentation experiments were performed by mixing the FLG stock with 10 mmol/L NaCl solution to yeild the initial FLG concentration of 1 mg/L. After settling for 7 d (a long enough period to reach equilibrium), the upper layer suspensions (i.e., 1/5 of the total volume) were deposited on mica plate, air dried and then analyzed by AFM. The size distribution of FLG suspension at the beginning of sedimentation experiment was also characterized by AFM as control.

2.4. Uptake experiments

Zebrafish embryos were exposed to FLG suspensions to compare the potential ecological effects of FLG differed in lateral size. Before the uptake experiments, prolonged sonication (up to 60 h) was conducted to prepare S-FLG stock suspension using the same procedures as the stock FLG. Size distribution and elemental composition of S-FLG were analyzed by

AFM and XPS, respectively. Fish embryo exposure experiment was conducted according to the OECD standard test protocol (OECD, 2013). Briefly, the FLG and S-FLG stock suspensions were diluted separately by clean water to yeild exposure concentration of (75 ± 1) μg/L (n=3). Zebrafish embryos at 2 h post fertilization were distributed in 96-well plates (one embryo per well); each well contained 100 μL of FLG or S-FLG suspension. After that, the embryos were cultured at (26 ± 1) °C for 12 h, 24 h, and 48 h. Triplicate experiments (n=100 embryos/ treatment/ replicate) were conducted. At each time point, one hundred embryos were removed, each embryo was washed three times with DI water. After this procedure, FLG aggregates were not visible on the membranes of the embryos, and contributions from the attached FLG to the total mass of FLG associated with the chorion are thus expected to be insignificant. Following the DI water rinse step, chorion and yolk in each embryo was carefully sepatated using the method described by Orlova et al. (2014). Once the chorion was pulled away, the yolk was able to freely swim out from the chorion. The collected chorions (or yolks) (n=100) were pooled and combusted using biological oxidation (OX-500, Zinser Analytic), and then the radioactivity was analyzed using LSC (Mao et al., 2016).

Another group of embryos was exposed to the S-FLG suspensions using the same procedure described above. At 48 h, the randomly selected embryos were removed and rinsed with 0.1 M phosphate buffered saline (PBS) buffer. The yolks were taken out of the embryos, rinsed with PBS buffer, and fixed with 3 % glutaraldehyde for 24 h, which was followed by a post-fixation step with 1.0 % osmium tetroxide for 1 h. After dehydration in a series of (50, 70, 80, 95, and 100) % ethanol, the samples were embedded with propylene oxide and epoxy mixture. Ultra-thin sections (the thickness of each section was about 50 nm to 60 nm) were placed on formvar-coated copper grids (300 mesh)(Kwon et al., 2015). The sections of the yolks were stained with uranyl acetate and lead citrate and observed using a FEI Tecnai TF20 high resolution transmission electron microscope (HRTEM) to verify the presence of S-FLG in the yolk.

2.5. DLVO interaction energy between FLG-FLG

According to the DLVO theory, the total interaction energy between particles can be defined as the sum of the van der Waals (VDW) attraction and the electrostatic double layer (EDL) repulsion (Elimelech, 1995). The FLG-FLG interaction energy profiles under different FLG and NaCl concentrations were calculated assuming plate-plate geometry (Elimelech, 1995; Gregory, 1981). Detailed equations and parameters are presented in the SI.

2.6. Statistical analysis

One-way ANOVA with Tukey's multiple comparison tests was used to determine the statistical differences in sedimentation rate constants and D_h values of FLG among different solution chemistries and to compare differences in FLG contents that accumulated by organisms. Statistical difference was set at $p < 0.05$.

3. Results and Discussion

3.1. Agglomeration of graphene at high concentrations

Cuvettes containing various concentrations (1 mg/L to 10 mg/L) of FLG dispersed in DI water are shown in Fig. 1a. Since all FLG suspensions were optically transparent, the DLS method was successfully used for measurement changes in the D_h of FLG as a function of time. The D_h values of FLG were relatively constant in DI water within 1 h at a concentration range of 1 mg/L to 3 mg/L, whereas FLG agglomerated within a few minutes at concentrations above 3 mg/L (Fig. 1b). This showed that the stability of FLG was much weaker than that of GO, which was stable in DI water at much higher concentrations (10 mg/L to 40 mg/L) (Chowdhury et al., 2013; Wu et al., 2013). For the dilute FLG suspensions (1 mg/L to 3 mg/L), the presence of Na^+ (e.g., 10 mmol/L) induced the formation of agglomerates (Fig. 1c). Notablely, the agglomeration was faster with increasing FLG concentration at the same IS. For instance, the initial agglomeration rate constant (k_a) (i.e., the initial rate of increase in D_h from $D_{h,initial}$ to$1.5D_{h,initial}$ with time) (Bouchard et al., 2012; Chowdhury et al., 2013; Holthoff et al., 1996) of 3 mg/L of FLG was (0.2300 ± 0.0003) nm/s in 1 mmol/L NaCl, which was 2.1 and 3.8 times higher than that of 2.5 mg/L ((0.110 ± 0.003) nm/s) and 1 mg/L ((0.060 ± 0.001) nm/s) of FLG, respectively. In addition, the k_a measured under diffusion-limited conditions increased proportionally with FLG concentration (R^2=0.9870) (Fig. S2). This suggests that a narrow FLG concentration range had a strong impact on the agglomeration behaviors.

Plots of attachment efficiency (α_a) as a function of NaCl concentration exhibit two distinct regions: a reaction-limited regime where α_a increases with IS at low IS, and a diffusion-limited regime in which α_a is independent of IS at higher NaCl concentrations (Fig. 1d). This indicates that the agglomeration of FLG is in general agreement with the DLVO theory (Chen and Elimelech, 2006; Chen et al., 2006). The intersection between the extrapolations through the reaction- and diffusion-limited regimes yielded CCC value (Chen and Elimelech, 2006; Elimelech, 1995). Unexpectedly, the CCC values were greatly affected by the concentrations of FLG, which were determined to be (1.550 ± 0.001) mmol/L, (5.18 ± 0.03) mmol/L, and (9.960 ± 0.004) mmol/L NaCl for 3 mg/L, 2.5 mg/L, and 1 mg/L of FLG, respectively. Likely mechanisms for this finding are discussed in later sections. As summarized in Table S2, these CCC values are much lower than the CCC values for C_{60} (120 mmol/L to 260 mmol/L NaCl) (Bouchard et al., 2009; Chen and Elimelech, 2006), CNTs (37 mmol/L to 210 mmol/L NaCl) (Sano et al., 2001; Smith et al., 2008; Yi and Chen, 2011), and GO (44 mmol/L to 188 mmol/L NaCl) (Chowdhury et al., 2013; Wu et al., 2013), indicating that the FLG is less stable. Since the surface oxygen content of CNMs has a great influence on their CCC values (Smith et al., 2009; Yi and Chen, 2011), the poorer stability of FLG may be attributed to its lower oxygen content (6 %) (Guo et al., 2013) than that of other CNMs, such as the oxidized CNTs (10.6 %) (Yi and Chen, 2011) and GO (60 %) (Chowdhury et al., 2015). Difference in particle size may also play an important role, but it is challenging to make direct comparisons among the nominal hydrodynamic diameter values of CNMs given their variable shapes.

3.2. Effects of mass concentration on attachment efficiency of graphene

The effect of particle concentration on the stability of colloids has been the subject of a number of studies (Hanus et al., 2001; Hsu and Liu, 1998; Tezak et al., 1951), but no study has yet focused on the CNMs. Agglomeration studies clearly showed that the effects of Na^+ on the FLG-FLG interaction followed the prediction of the DLVO theory (Chen and Elimelech, 2006; Chen et al., 2006), but the attachment efficiency was largely different in a narrow FLG concentration (i.e., 1 mg/L to 3 mg/L) under reaction-limited conditions (e.g., 1 mmol/L NaCl). We assume that the disparity in attachment efficiency among these FLG concentrations should be caused by the difference in total interaction energy. Particle size and zeta potential are key parameters that control the total interaction energy of colloids according to the DLVO theory (Elimelech, 1995; Gregory, 1981). Since the initial D_h values of FLG under these concentrations were not significantly different ($p > 0.05$) (Table S3), the effects of Na^+ on charge screening may be greater at higher FLG concentrations. So that the VDW attraction overweights the EDL repulsion more readily, allowing the FLG sheets to approach closer. Electrophoretic mobility measurements showed that the absolute values of EPM in NaCl solutions (0 mmol/L to 100 mmol/L) gradually decreased as the FLG concentration increased from 1 mg/L to 10 mg/L (Fig. S3). For example, from 1 mg/L to 3 mg/L, the absolute values of EPM decreased from $(-2.03 \pm 0.05)\times10^{-8}$ m^2/Vs to $(-1.49 \pm 0.06)\times10^{-8}$ m^2/Vs in 1 mmol/L NaCl. This concentration-dependent trending in the EPM was observed for titanium dioxide, polyurethane, and hexadecane particles (Kaszuba et al., 2010; Medrzycka, 1991). The mechanism by which concentration affects the EPM of FLG is unclear, but it can be sure that obscuration of light transmission is negligible as the intensity of scattered light being detected was still very high at FLG concentration of 10 mg/L. The DLVO interaction energy profiles between FLG-FLG as functions of FLG and NaCl concentrations are shown in Table S4 and Fig. S4. At a given FLG concentration, the DLVO calculations predict the presence of deepened secondary energy minima at higher NaCl concentration (from 0.5 mmol/L to 10 mmol/L), thus resulting in greater particle collision and attachment as observed from the agglomeration experiments. An increase in the FLG concentration (from 1 mg/L to 3 mg/L) led to higher secondary energy minima at 5 mmol/L and 10 mmol/L NaCl, indicating that FLG particles agglomerate more readily in the more concentrated suspensions as a result of the increased attractive forces. This is helpful for explanation the observed faster agglomeration at 3 mg/L of FLG than that for 2 mg/L and 1 mg/L of FLG at same IS.

3.3. Long-term stability of graphene at low concentrations

To test the stability of FLG at more environmentally relevant concentrations below the DLS detection limit and for longer time periods (7 d to 28 d), sedimentation experiments were conducted using lower FLG concentrations (107 μg/L to 2 μg/L). During the first 60 minutes, the concentrations of FLG remained constant and were not significantly different ($p > 0.05$) in varying NaCl solutions (0 mmol/L to 1000 mmol/L) (Fig. S5). Thereafter, the settling profiles of the FLG (Fig. 2a) exhibited exponential decays and were well fitted by a first-order model (detailed procedures and results are shown in the SI and Table S5), a model which has also recently been applied to fit the sedimentation kinetics of other nanomaterials (Brunelli et al., 2013; Markus et al., 2015). The sedimentation rate constants (k_s) of FLG (107 μg/L) increased with greater IS at low NaCl concentrations (from (0.68 ± 0.08) d^{-1} at 0

mmol/L to (1.3 ± 0.2) d^{-1} at 10 mmol/L; uncertainties of k_s indicate standard error values), but did not significantly increase ($p > 0.05$) when the NaCl concentration was higher than 10 mmol/L (i.e., 10 mmol/L compared to 50 mmol/L or 500 mmol/L NaCl) (Fig. 2b). Similar effects of Na^+ on the stability of FLG were also observed for FLG concentrations of 11 μg/L and 2 μg/L. Therefore, the agglomeration of FLG varied with IS also in a manner consistent with the DLVO theory under these low FLG concentrations. It is worth noting that particle concentration had a greater effect on the sedimentaion than the IS. At a given NaCl concentration (i.e., 10 mmol/L), the k_s of 2 μg/L of FLG was a factor of 13.5 and 2.7 times smaller than that of FLG at higher concentrations of 107 μg/L and 11 μg/L, respectively (Table S5). This result is also consistent with our earlier observations that the agglomeration of FLG was faster at higher FLG concentrations (i.e., 3 mg/L compared to 2.5 mg/L or 1 mg/L) (Fig. 1c).

The sedimentation kinetics of FLG in eight ambient waters (pH = 7.7 ± 0.4; details for water characteristics are provided in Table S6) showed that water type had a notable influence on the stability of FLG (Fig. 3a and b). Destabilization of FLG occurred quickly in the East China Sea water and the influent and treated effluent from a wastewater treatment plant (WWTP); the concentrations of FLG (50 μg/L) were sharply reduced bŷ 71 %, ~ 43 %, and ~ 40 % within 1 d, respectively. In comparison, the FLG underwent slow agglomeration in other five freshwaters and underground waters; approximately 42 % – 65 % of FLG (50 μg/L) remained suspended after one week, the lowest sedimentation was observed for the Qinghai Lake water for which more than 70 % of FLG (4 μg/L) remained in aqueous phase after 28 d. Since the insoluble fraction was removed by filtration with a 0.22 μm cellulose acetate membrane, sedimentation was mainly affected by the IS of the waters. Plots of the k_s versus the total IS (i.e., the sum of the IS of F^-, Cl^-, NO_3^-, SO_4^{2-}, K^+, Na^+, Ca^{2+}, and Mg^{2+}) of the waters are shown in Fig. S6c. The k_s values of FLG were constant under lower total IS (0.234 mmol/L to 4.79 mmol/L), but significantly increased ($p < 0.05$) when the total IS approached 10 mmol/L. The presence of NOM (2.1 mg TOC/L to 34 mg TOC/L) had a stabilizing effect on FLG in the low IS freshwaters and ground waters. The FLG had a high affinity for SRNOM at 10 mmol/L NaCl (details of adsorption experiments are provided in SI) (Fig. S6). Adsorption of NOM macromolecules onto FLG resulted in steric and electrostatic repulsions (the EPM values of FLG were more negative with addition of SRNOM compared to NaCl alone (Fig. S7a), which effectively retarded the agglomeration and sedimentation of FLG in 10 mmol/L NaCl (Fig. S7b and 2c); the CCC for NaCl was increased by 9.5 times from (9.960 ± 0.004) mmol/L to (95.00 ± 0.09) mmol/L with addition of SRNOM (0.57 mg TOC/L) (Fig. 1d). The sedimentation of FLG in ambient waters also showed a strong dependence on FLG concentration. At a lower FLG concentration (4 μg/L), the k_s values of FLG in all water samples were reduced by 1.7 to 4.4 times compared to a higher FLG concentration (50 μg/L) (Table S6).

3.4. Size distribution of suspended graphene

The long-term stability studies further verified that the mass concentration of FLG played an important role in affecting salt-induced agglomeration and settling. At higher concentrations, settling of a single particle is often impacted by other particles. The formation of agglomerates accelerates the sedimentation of the colliding particles and reduces the number

of primary particle and total particle. For FLG suspensions with nonuniform size distribution, small FLG sheets often diffuse faster than the larger ones according to the Stokes-Einstein equation (Cho et al., 2011). It is possible that agglomeration resulting from collisions between small-small or small-larger FLG sheets will reduce the number of small particles. To confirm this hypothesis, the lateral size of FLG (1 mg/L, in 10 mmol/L NaCl) before and after sedimentation for 7 d was characterized by AFM. As shown in Fig. 4a and b, settling process did not significantly affect the thickness of FLG, which was measured to be (0.34–4.17) nm and (0.33–3.22) nm at 0 d and 7 d, respectively; 71 % (0 d) or 69 % (7 d) of total count was in the range of (0.5–1) nm. However, sedimentation led to significant reduction in the total particle number of FLG and removal of larger FLG sheets. The width of size distribution of FLG was shortened from (20–993) nm (0 d) to (22–569) nm (7 d), as 4.4 % of total counted FLG ranging from 575 nm to 975 nm had settled out of water. The AFM results confirmed that 18 % of total counted FLG was in the range of (25–50) nm at the beginning of sedimentation experiment (0 d). After settling for 7 d, the fraction of these small FLG in aqueous phase was decreased to 6 %. When the number of primary particles decreases to a threhold at which the motion of a single particle is less likely affected by the surrounding particles, the small and large FLG sheets may settle independently, the agglomeration and settling of primary particles slow down. Thus, the normalized concentrations (i.e., C/C_0) of FLG were relatively constant at same IS from 3 d to 7 d at concentration of 107 μg/L (Fig. 2a). It is worth noting that FLG will take longer time to achieve the same degree of agglomeration under more dilute conditions (e.g., 11 μg/L and 2 μg/L). In such cases, decreasing mass concentration leads to slow removal and a longer persistence of the small FLG (i.e., 25 nm to 50 nm) in water column and higher potential of exposure to aquatic organism.

3.5. Size-dependent uptake of graphene by zebrafish embryo

Size dependence of cellular uptake, cytoxicity, and antimicrobial activity have been observed for GO (Ma et al., 2015; Mu et al., 2012; Perreault et al., 2015). It is still not known whether uptake of pristine graphene by ecological receptor is size dependent. To explore impact of lateral size on biological uptake of FLG and to avoid interference from Na^+, we prepared S-FLG by prolonged sonication (up to 60 h). Prolonged sonication did not significantly change the elemental composition of FLG (data not shown), but greatly increased the percentage of (25–50) nm FLG from 18 % to 88 % on the basis of AFM results (Fig. S8). In addition, analysis of the extracts using LSC and gas chromatography-mass spectrometry (GC-MS) did not show a significant increase in the radioactivity or obvious chemical peaks in GC-MS chromatograms of the extracted solutions, indicating that degradation products were not formed from the prolonged sonication processes of FLG. Uptake of FLG and S-FLG by zebrafish embryos was further investigated. The distribution of FLG within the zebrafish embryos varied with the lateral size (Fig. 5a). When exposed to FLG for 12 h–48 h, 85 % – 98 % of the total mass of the accumulated FLG (i.e., the sum of the FLG contents in the choroin and the yolk) was in the choroin and few of them was detected in the yolk. In comparison, the contents of S-FLG in the choroin were significantly enhanced by 3.7, 3.0, and 1.6 times at 12 h, 24 h, and 48 h, respectively. Moreover, 16 % – 21 % of the total mass of the accumulated S-FLG passed the choroin to the yolk. To confirm the presence of the S-FLG in the yolk, ultra-thin sections of the yolk were observed through HRTEM (Fig. 5b),

which shows visible ordered graphite lattices with interlayer distance of 0.342 nm that is equal to the reported interlayer distance of graphite (Deng et al., 2011). Well-defined diffraction spots that represent the crystalline structure of graphene (Brown et al., 2014) were also observed in the fourier transfer image of Fig. 5b. These observations demonstrated that decrease in size greatly enhanced the membrane penetration ability of FLG. The microstructure of the chorion may be a decisive factor affecting the transmembrane transport of FLG. Zebrafish chorion consists of three layers that are pierced by cone-shaped pore canals, given the narrow diameter (500 nm to 700 nm) (Rawson et al., 2000), these pores may restrict the uptake of large particles that presented in FLG suspension. As mentioned previously, large FLG with lateral size ranging from 575 nm to 975 nm accounted for 4.4 % of the total counted FLG sheets (Fig. 4c). Because the mass of FLG particles is proportional to the square of diameter, a 500 nm particle would have a factor of 100 more mass than a 50 nm particle (assuming similar thickness). Unlike S-FLG, the mass of the large particles mainly contributed to the total mass of FLG. The limited bioaccessbility of these large particles impeded the accumulation of FLG in the yolk. In addition, the S-FLG may have different agglomeration behavior from FLG, the more slowly S-FLG agglomerated, the more small particles would be taken up by embyos.

4. Conclusion

The agglomeration behavior of graphene will dictate its transport and fate in the environment. Our results show that the concentration of FLG is a key factor in its agglomeration and stability in aqueous media, but one that was often overlooked in previous studies. At a given IS, the agglomeration rates decreased with dilution of FLG suspensions from 3 mg/L to 0.1 mg/L, and the settling of FLG was substantially slower at concentrations lower than 0.1 mg/L. Although cations induced fast agglomeration when the IS approached 10 mmol/L NaCl, the presence of NOM effectively improved the stability of FLG by electrostatic and steric interactions. Long-term stability studies suggest that FLG agglomeration at low concentrations is expected in freshwater, but slow sedimentation may result in continued FLG exposure to pelagic organisms. FLG entering seawater will be removed from the water column at a rapid rate, and marine benthos may be at higher risk of exposure than aquatic organisms. In addition, more attention should be paid to evaluating the environmental risk of small FLG particles in consideration of their persistence at low concentrations and their high bioaccumulation behaviors. The results from this study will aid in the choice of test media for aquatic toxicity testing because exposing the organisms to a constant nanomaterial concentration by minimizing agglomeration and sedimentation is typically a goal of these tests.

Supplementary Material

Refer to Web version on PubMed Central for supplementary material.

Acknowledgments

We acknowledge the financial support from the National Natural Science Foundation of China (21377049, 21237001, and 21607072) and a Foundation for the Author of National Excellent Doctoral Dissertation of PR China (201355). Certain commercial equipment, instruments and materials are identified to specify experimental

procedures as completely as possible. In no case does such identification imply a recommendation or endorsement by the National Institute of Standards and Technology nor does it imply that any of the materials, instruments or equipment identified are necessarily the best available for the purpose.

Appendix A. Supplementary data

Additional details of experimental methods and results as well as other supporting tables and figures.

References

Akkanen J, Penttinen S, Haitzer M, Kukkonen JVK. Bioavailability of atrazine, pyrene and benzo[a]pyrene in European river waters. Chemosphere. 2001; 45:453–462. [PubMed: 11680741]

Anderson R, Barron AR. Reaction of hydroxyfullerene with metal salts: A route to remediation and immobilization. J Am Chem Soc. 2005; 127:10458–10459. [PubMed: 16045311]

Batley GE, Kirby JK, McLaughlin MJ. Fate and risks of nanomaterials in aquatic and terrestrial environments. Acc Chem Res. 2012; 46:854–862. [PubMed: 22759090]

Bouchard D, Ma X, Isaacson C. Colloidal properties of aqueous fullerenes: Isoelectric points and aggregation kinetics of C_{60} and C_{60} derivatives. Environ Sci Technol. 2009; 43:6597–6603. [PubMed: 19764223]

Bouchard D, Zhang W, Powell T, Rattanaudompol Us. Aggregation kinetics and transport of single-walled carbon nanotubes at low surfactant concentrations. Environ Sci Technol. 2012; 46:4458–4465. [PubMed: 22443301]

Brown L, Lochocki EB, Avila J, Kim CJ, Ogawa Y, Havener RW, Kim DK, Monkman EJ, Shai DE, Wei HI, Levendorf MP, Asensio M, Shen KM, Park J. Polycrystalline graphene with single crystalline electronic structure. Nano Lett. 2014; 14:5706–5711. [PubMed: 25207847]

Brunelli A, Pojana G, Callegaro S, Marcomini A. Agglomeration and sedimentation of titanium dioxide nanoparticles ($nTiO_2$) in synthetic and real waters. J Nanopart Res. 2013; 15:1–10.

Bussy C, Ali-Boucetta H, Kostarelos K. Safety considerations for graphene: Lessons learnt from carbon nanotubes. Acc Chem Res. 2013; 46:692–701. [PubMed: 23163827]

Chen KL, Elimelech M. Aggregation and deposition kinetics of fullerene (C_{60}) nanoparticles. Langmuir. 2006; 22:10994–11001. [PubMed: 17154576]

Chen KL, Elimelech M. Interaction of fullerene (C_{60}) nanoparticles with humic acid and alginate coated silica surfaces: Measurements, mechanisms, and environmental implications. Environ Sci Technol. 2008; 42:7607–7614. [PubMed: 18983082]

Chen KL, Elimelech M. Relating colloidal stability of fullerene (C_{60}) nanoparticles to nanoparticle charge and electrokinetic properties. Environ Sci Technol. 2009; 43:7270–7276. [PubMed: 19848133]

Chen KL, Mylon SE, Elimelech M. Aggregation kinetics of alginate-coated hematite nanoparticles in monovalent and divalent electrolytes. Environ Sci Technol. 2006; 40:1516–1523. [PubMed: 16568765]

Cho EC, Zhang Q, Xia Y. The effect of sedimentation and diffusion on cellular uptake of gold nanoparticles. Nat Nanotechnol. 2011; 6:385–391. [PubMed: 21516092]

Chowdhury I, Duch MC, Mansukhani ND, Hersam MC, Bouchard D. Colloidal properties and stability of graphene oxide nanomaterials in the aquatic environment. Environ Sci Technol. 2013; 47:6288–6296. [PubMed: 23668881]

Chowdhury I, Mansukhani ND, Guiney LM, Hersam MC, Bouchard D. Aggregation and stability of reduced graphene oxide: Complex roles of divalent cations, pH, and natural organic matter. Environ Sci Technol. 2015; 49:10886–10893. [PubMed: 26280799]

Deng D, Pan X, Yu L, Cui Y, Jiang Y, Qi J, Li W, Fu Q, Ma X, Xue Q, Sun G, Bao X. Toward N-doped graphene via solvothermal synthesis. Chem Mater. 2011; 23:1188–1193.

Duch MC, Budinger GRS, Liang YT, Soberanes S, Urich D, Chiarella SE, Campochiaro LA, Gonzalez A, Chandel NS, Hersam MC, Mutlu GM. Minimizing oxidation and stable nanoscale dispersion

improves the biocompatibility of graphene in the lung. Nano Lett. 2011; 11:5201–5207. [PubMed: 22023654]

Eda G, Fanchini G, Chhowalla M. Large-area ultrathin films of reduced graphene oxide as a transparent and flexible electronic material. Nat Nanotechnol. 2008; 3:270–274. [PubMed: 18654522]

Elimelech, MGJ., Jia, X., Williams, RA. Particle deposition and aggregation: Measurement, modelling and simulation. Oxford; U.K.: 1995.

Feng Y, Lu K, Mao L, Guo X, Gao S, Petersen EJ. Degradation of ^{14}C-labeled few layer graphene via Fenton reaction: Reaction rates, characterization of reaction products, and potential ecological effects. Water Res. 2015; 84:49–57. [PubMed: 26210029]

Geim AK. Graphene: Status and prospects. Science. 2009; 324:1530–1534. [PubMed: 19541989]

Gregory J. Approximate expressions for retarded van der waals interaction. J Colloid Interface Sci. 1981; 83:138–145.

Guo X, Dong S, Petersen EJ, Gao S, Huang Q, Mao L. Biological uptake and depuration of radio-labeled graphene by *Daphnia magna*. Environ Sci Technol. 2013; 47:12524–12531. [PubMed: 24099417]

Hanus LH, Hartzler RU, Wagner NJ. Electrolyte-induced aggregation of acrylic latex. 1. Dilute particle concentrations. Langmuir. 2001; 17:3136–3147.

Holthoff H, Egelhaaf SU, Borkovec M, Schurtenberger P, Sticher H. Coagulation rate measurements of colloidal particles by simultaneous static and dynamic light scattering. Langmuir. 1996; 12:5541–5549.

Hsu JP, Liu BT. Critical coagulation concentration of a colloidal suspension at high particle concentrations. J Phys Chem B. 1998; 102:334–337.

Hu X, Mu L, Kang J, Lu K, Zhou R, Zhou Q. Humic acid acts as a natural antidote of graphene by regulating nanomaterial translocation and metabolic fluxes in vivo. Environ Sci Technol. 2014; 48:6919–6927. [PubMed: 24857237]

Hu X, Zhou M, Zhou Q. Ambient water and visible-light irradiation drive changes in graphene morphology, structure, surface chemistry, aggregation, and toxicity. Environ Sci Technol. 2015; 49:3410–3418. [PubMed: 25686198]

Huang G, Guo H, Zhao J, Liu Y, Xing B. Effect of co-existing kaolinite and goethite on the aggregation of graphene oxide in the aquatic environment. Water Res. 2016; 102:313–320. [PubMed: 27379727]

Kaszuba M, Corbett J, Watson FM, Jones A. High-concentration zeta potential measurements using light-scattering techniques. Philos transact A Math Phys Eng Sci. 2010; 368:4439–4451.

Konkena B, Vasudevan S. Understanding aqueous dispersibility of graphene oxide and reduced gaphene oxide through pKa measurements. J Phys Chem Lett. 2012; 3:867–872. [PubMed: 26286412]

Kwon D, Nho HW, Yoon TH. Transmission electron microscopy and scanning transmission X-ray microscopy studies on the bioaccumulation and tissue level absorption of TiO_2 nanoparticles in *Daphnia magna*. J Nanosci Nanotechnol. 2015; 15:4229–4238. [PubMed: 26369034]

Lowry GV, Gregory KB, Apte SC, Lead JR. Transformations of nanomaterials in the environment. Environ Sci Technol. 2012; 46:6893–6899. [PubMed: 22582927]

Lu K, Huang Q, Wang P, Mao L. Physicochemical changes of few-layer graphene in peroxidase-catalyzed reactions: Characterization and potential ecological effects. Environ Sci Technol. 2015; 49:8558–8565. [PubMed: 26086574]

Ma J, Liu R, Wang X, Liu Q, Chen Y, Valle RP, Zuo YY, Xia T, Liu S. Crucial role of lateral size for graphene oxide in activating macrophages and stimulating pro-inflammatory responses in cells and animals. ACS Nano. 2015; 9:10498–10515. [PubMed: 26389709]

Mao L, Hu M, Pan B, Xie Y, Petersen EJ. Biodistribution and toxicity of radio-labeled few layer graphene in mice after intratracheal instillation. Part Fibre Toxicol. 2016; 13:1–12. [PubMed: 26746196]

Markus AA, Parsons JR, Roex EWM, de Voogt P, Laane RWPM. Modeling aggregation and sedimentation of nanoparticles in the aquatic environment. Sci Total Environ. 2015:506–507.

Maurer-Jones MA, Gunsolus IL, Murphy CJ, Haynes CL. Toxicity of engineered nanoparticles in the environment. Anal Chem. 2013; 85:3036–3049. [PubMed: 23427995]

Medrzycka KB. The effect of particle concentration on zeta potential in extremely dilute solutions. Colloid Polym Sci. 1991; 269:85–90.

Mu Q, Su G, Li L, Gilbertson BO, Yu LH, Zhang Q, Sun YP, Yan B. Size-dependent cell uptake of protein-coated graphene oxide nanosheets. ACS Appl Mater Inter. 2012; 4:2259–2266.

Novoselov KS, Falko VI, Colombo L, Gellert PR, Schwab MG, Kim K. A roadmap for graphene. Nature. 2012; 490:192–200. [PubMed: 23060189]

Novoselov KS, Geim AK, Morozov SV, Jiang D, Zhang Y, Dubonos SV, Grigorieva IV, Firsov AA. Electric field effect in atomically thin carbon films. Science. 2004; 306:666–669. [PubMed: 15499015]

OECD. Fish embryo acute toxicity (FET) test. OECD Guidelines for the testing of Chemicals. 2013; 236

Orlova VV, van den Hil FE, Petrus-Reurer S, Drabsch Y, ten Dijke P, Mummery CL. Generation, expansion and functional analysis of endothelial cells and pericytes derived from human pluripotent stem cells. Nature Protoc. 2014; 9:1514–1531. [PubMed: 24874816]

Pakarinen K, Petersen EJ, Alvila L, Waissi-Leinonen GC, Akkanen J, Leppänen MT, Kukkonen JVK. A screening study on the fate of fullerenes (nC_{60}) and their toxic implications in natural freshwaters. Environ Toxicol Chem. 2013; 32:1224–1232. [PubMed: 23404765]

Perreault F, de Faria AF, Nejati S, Elimelech M. Antimicrobial properties of graphene oxide nanosheets: Why size matters. ACS Nano. 2015; 9:7226–7236. [PubMed: 26091689]

Petersen EJ, Diamond SA, Kennedy AJ, Goss GG, Ho K, Lead J, Hanna SK, Hartmann NB, Hund-Rinke K, Mader B, Manier N, Pandard P, Salinas ER, Sayre P. Adapting OECD aquatic toxicity tests for use with manufactured nanomaterials: Key issues and consensus recommendations. Environ Sci Technol. 2015; 49:9532–9547. [PubMed: 26182079]

Petersen EJ, Henry TB. Methodological considerations for testing the ecotoxicity of carbon nanotubes and fullerenes: Review. Environ Toxicol Chem. 2012; 31:60–72. [PubMed: 21994158]

Ramanathan T, Abdala AA, Stankovich S, Dikin DA, Herrera Alonso M, Piner RD, Adamson DH, Schniepp HC, Chen X, Ruoff RS, Nguyen ST, Aksay IA, Prud'Homme RK, Brinson LC. Functionalized graphene sheets for polymer nanocomposites. Nat Nanotechnol. 2008; 3:327–331. [PubMed: 18654541]

Rawson DM, Zhang T, Kalicharan D, Jongebloed WL. Field emission scanning electron microscopy and transmission electron microscopy studies of the chorion, plasma membrane and syncytial layers of the gastrula-stage embryo of the zebrafish *Brachydanio rerio*: A consideration of the structural and functional relationships with respect to cryoprotectant penetration. Aquacult Res. 2000; 31:325–336.

Sano M, Okamura J, Shinkai S. Colloidal nature of single-walled carbon nanotubes in electrolyte solution: The Schulze–Hardy rule. Langmuir. 2001; 17:7172–7173.

Schedin F, Geim AK, Morozov SV, Hill EW, Blake P, Katsnelson MI, Novoselov KS. Detection of individual gas molecules adsorbed on graphene. Nat Mater. 2007; 6:652–655. [PubMed: 17660825]

Schinwald A, Murphy FA, Jones A, MacNee W, Donaldson K. Graphene-based nanoplatelets: A new risk to the respiratory system as a consequence of their unusual aerodynamic properties. ACS Nano. 2012; 6:736–746. [PubMed: 22195731]

Seabra AB, Paula AJ, de Lima R, Alves OL, Durán N. Nanotoxicity of graphene and graphene oxide. Chem Res Toxicol. 2014; 27:159–168. [PubMed: 24422439]

Segal M. Selling graphene by the ton. Nat Nanotechnol. 2009; 4:612–614. [PubMed: 19809441]

Silva T, Pokhrel LR, Dubey B, Tolaymat TM, Maier KJ, Liu X. Particle size, surface charge and concentration dependent ecotoxicity of three organo-coated silver nanoparticles: Comparison between general linear model-predicted and observed toxicity. Sci Total Environ. 2014:468–469. [PubMed: 24742557]

Smith B, Wepasnick K, Schrote KE, Bertele AR, Ball WP, O'Melia C, Fairbrother DH. Colloidal properties of aqueous suspensions of acid-treated, multi-walled carbon nanotubes. Environ Sci Technol. 2008; 43:819–825.

Smith B, Wepasnick K, Schrote KE, Cho HH, Ball WP, Fairbrother DH. Influence of surface oxides on the colloidal stability of multi-walled carbon nanotubes: A structure–property relationship. Langmuir. 2009; 25:9767–9776. [PubMed: 19583226]

Stankovich S, Dikin DA, Dommett GHB, Kohlhaas KM, Zimney EJ, Stach EA, Piner RD, Nguyen ST, Ruoff RS. Graphene-based composite materials. Nature. 2006; 442:282–286. [PubMed: 16855586]

Tezak N, Matijevic E, Schulz K. Coagulation of hydrophobic sols in statu nascendi. II. Effect of the concentration of the sol and of the stabilizing ion on the coagulation of silver chloride, silver bromide, and silver iodide. J Phys Colloid Chem. 1951; 55:1567–1576.

Wang X, Zhi L, Müllen K. Transparent, conductive graphene electrodes for dye-sensitized solar cells. Nano Lett. 2008; 8:323–327. [PubMed: 18069877]

Wu L, Liu L, Gao B, Muñoz-Carpena R, Zhang M, Chen H, Zhou Z, Wang H. Aggregation kinetics of graphene oxides in aqueous solutions: Experiments, mechanisms, and modeling. Langmuir. 2013; 29:15174–15181. [PubMed: 24261814]

Yang K, Wan J, Zhang S, Zhang Y, Lee ST, Liu Z. In vivo pharmacokinetics, long-term biodistribution, and toxicology of PEGylated graphene in mice. ACS Nano. 2011; 5:516–522. [PubMed: 21162527]

Yang K, Zhang S, Zhang G, Sun X, Lee ST, Liu Z. Graphene in mice: Ultrahigh in vivo tumor uptake and efficient photothermal therapy. Nano Lett. 2010; 10:3318–3323. [PubMed: 20684528]

Yi P, Chen KL. Influence of surface oxidation on the aggregation and deposition kinetics of multiwalled carbon nanotubes in monovalent and divalent electrolytes. Langmuir. 2011; 27:3588–3599. [PubMed: 21355574]

Zhang Y, Ali SF, Dervishi E, Xu Y, Li Z, Casciano D, Biris AS. Cytotoxicity effects of graphene and single-wall carbon nanotubes in neural phaeochromocytoma-derived PC12 cells. ACS Nano. 2010; 4:3181–3186. [PubMed: 20481456]

Zhao CM, Wang WX. Size-dependent uptake of silver nanoparticles in *Daphnia magna*. Environ Sci Technol. 2012; 46:11345–11351. [PubMed: 22974052]

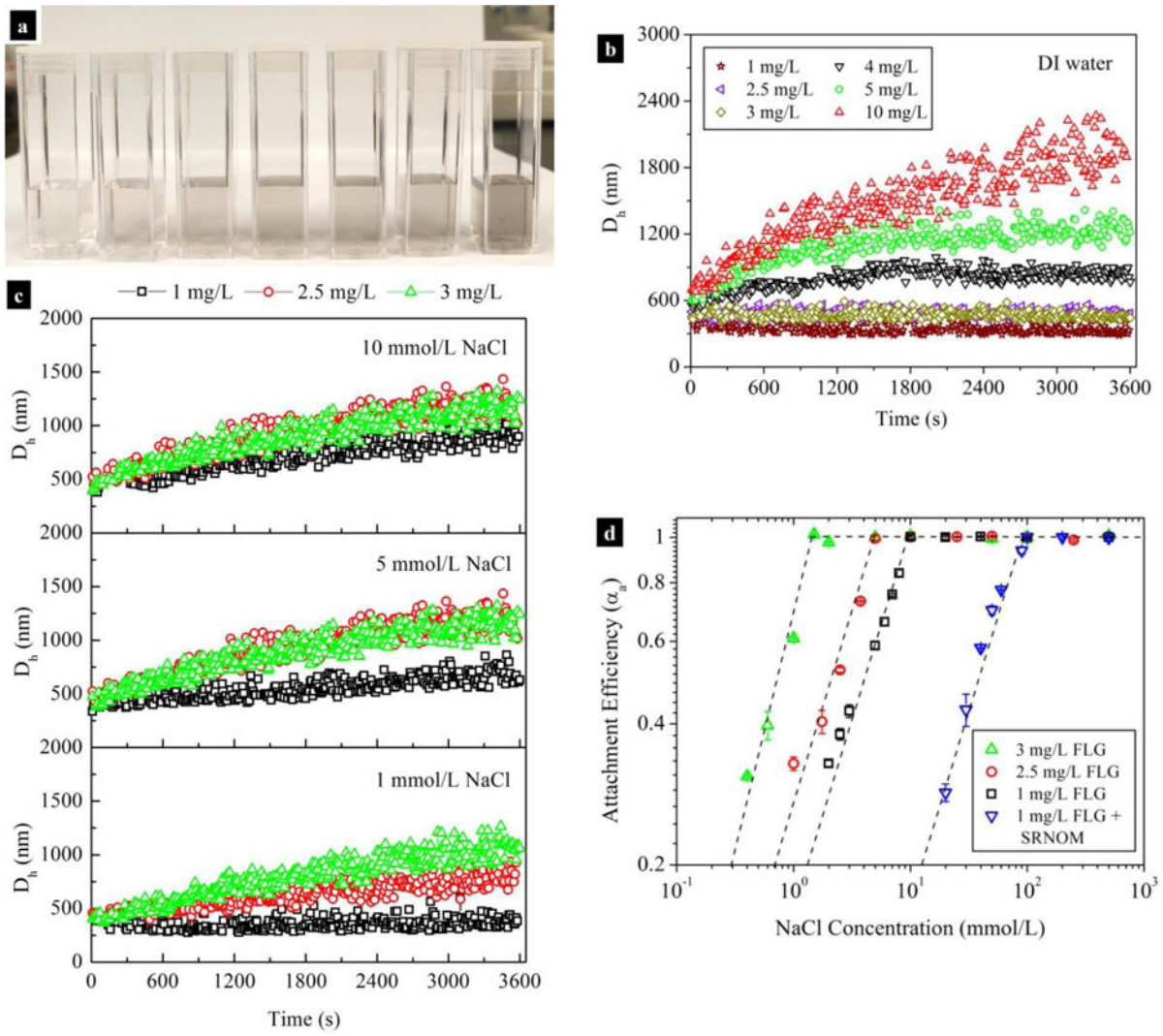

Fig. 1.

(a) Photograph of cuvettes containing various concentrations of FLG dispersed in DI water. Agglomeration profiles of FLG in DI water (b) or NaCl solutions (c) at various FLG concentrations at pH 7.0. Attachment efficiencies (d) of FLG determined at different FLG concentrations as a function of NaCl concentrarion (pH 7.0) in the absence and presence of 0.57 mg TOC/L SRNOM; data points are mean and standard deviation values that calculated from triplicate samples.

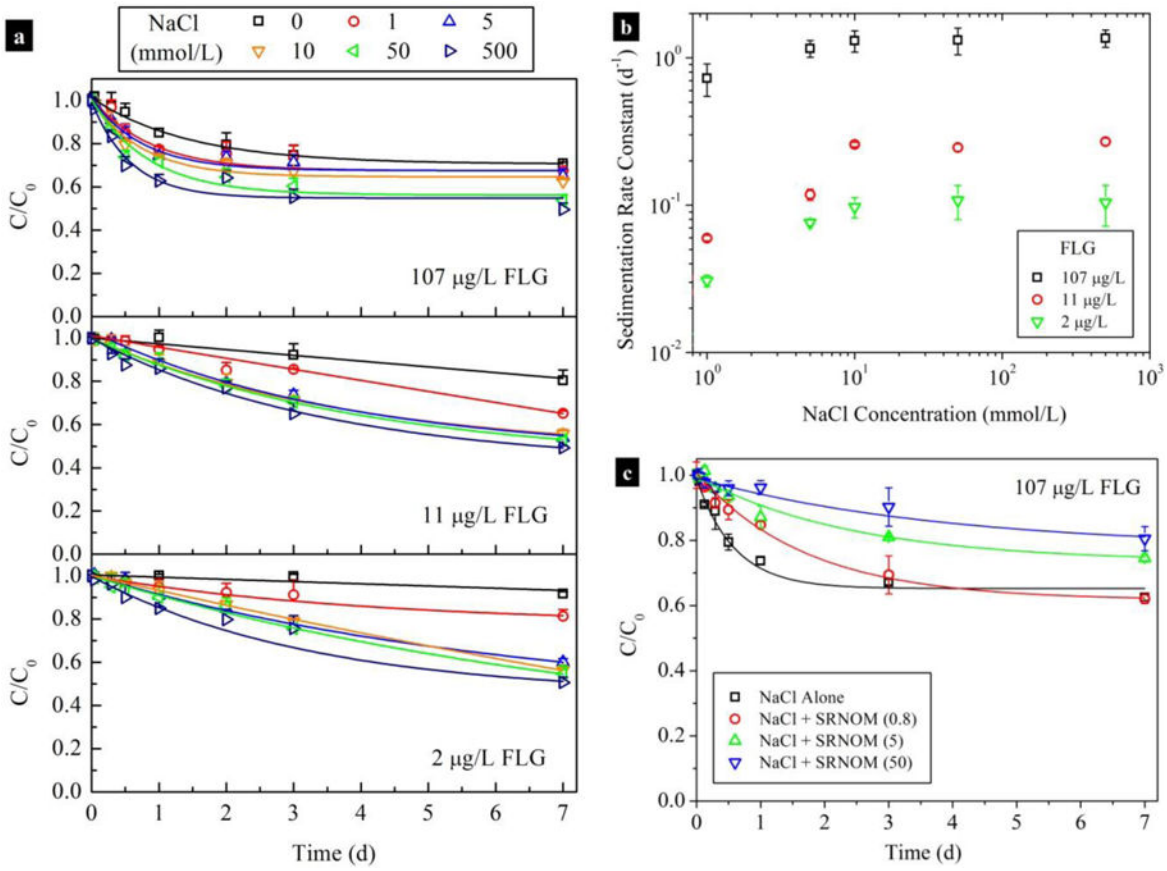

Fig. 2.

(a) Normalized FLG concentration suspended in NaCl solution at three different initial concentrations (107±3, 10.7±0.4, and 1.980±0.008) μg/L (n=3; uncertainties indicate standard deviation values). Sedimentation rate constants (b) of FLG as a function of NaCl concentration at initial FLG concentrations of (107±3, 10.7±0.4, and 1.980±0.008) μg/L (n=3); data points are mean and standard error values that obtained from Table S5. (c) Stability of FLG in 10 mmol/L NaCl in the absence and presence of SRNOM. The C/C_0 values are mean and standard deviation values that calculated from triplicate samples.

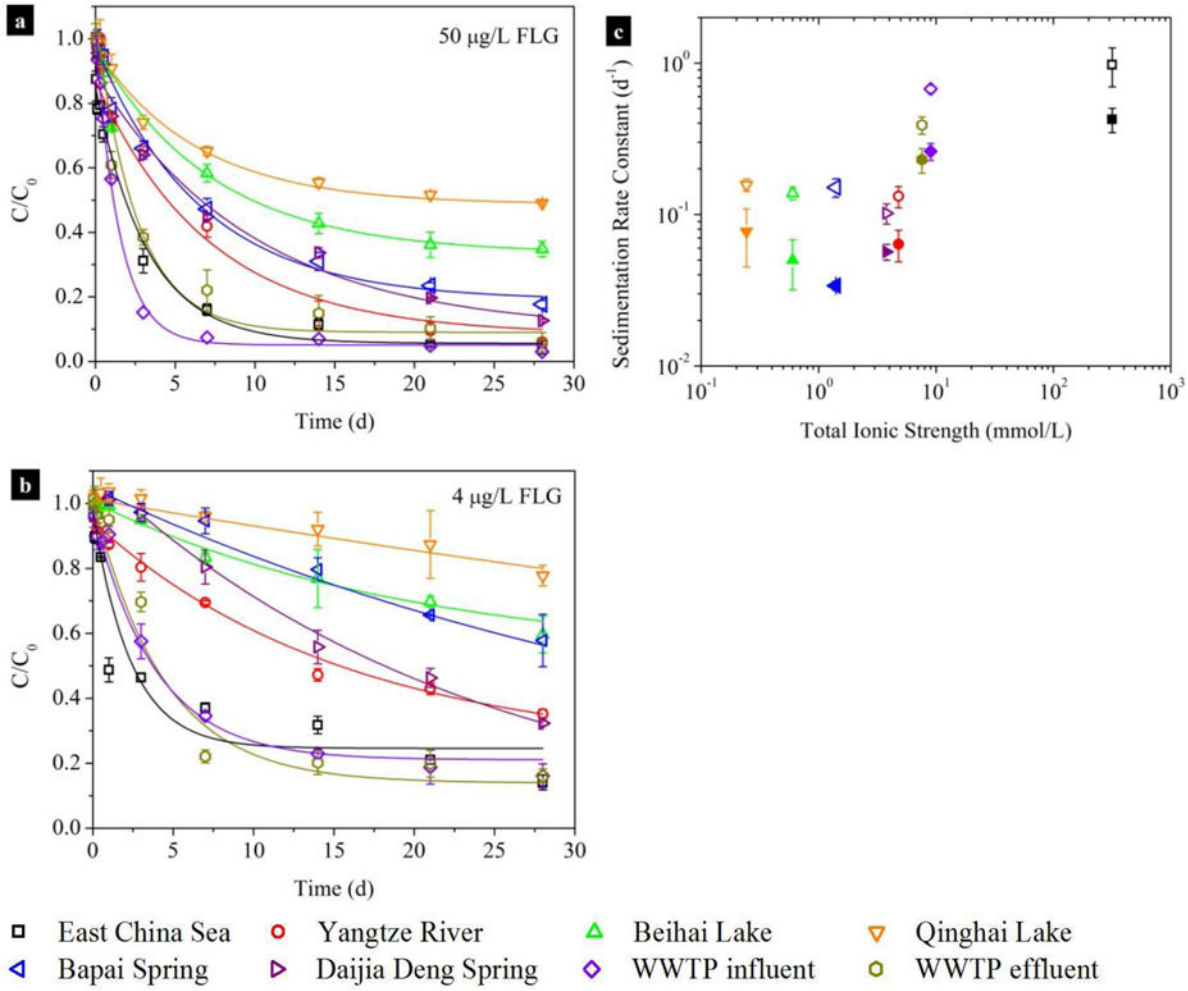

Fig. 3.

Long-term stability of FLG in ambient waters and wastewater samples from a municipal wastewater treatment plant (WWTP). Normalized FLG concentrations in different types of water, the initial FLG concentration was 50 μg/L (50 ± 2 μg/L, n=3) (a) and 4 μg/L (3.90 ± 0.03 μg/L, n=3) (b), respectively. Data points are mean and standard deviation values that calculated from triplicate samples. Sedimentation rate constants (c) of FLG at initial concentrations of 50 μg/L (open symbols) and 4 μg/L (solid symbols) as a function of total ionic strength of the water samples. Data points are mean and standard error values that obtained from Table S7. Details for water sampling locations and water characteristics are provided in Table S1 and Table S6.

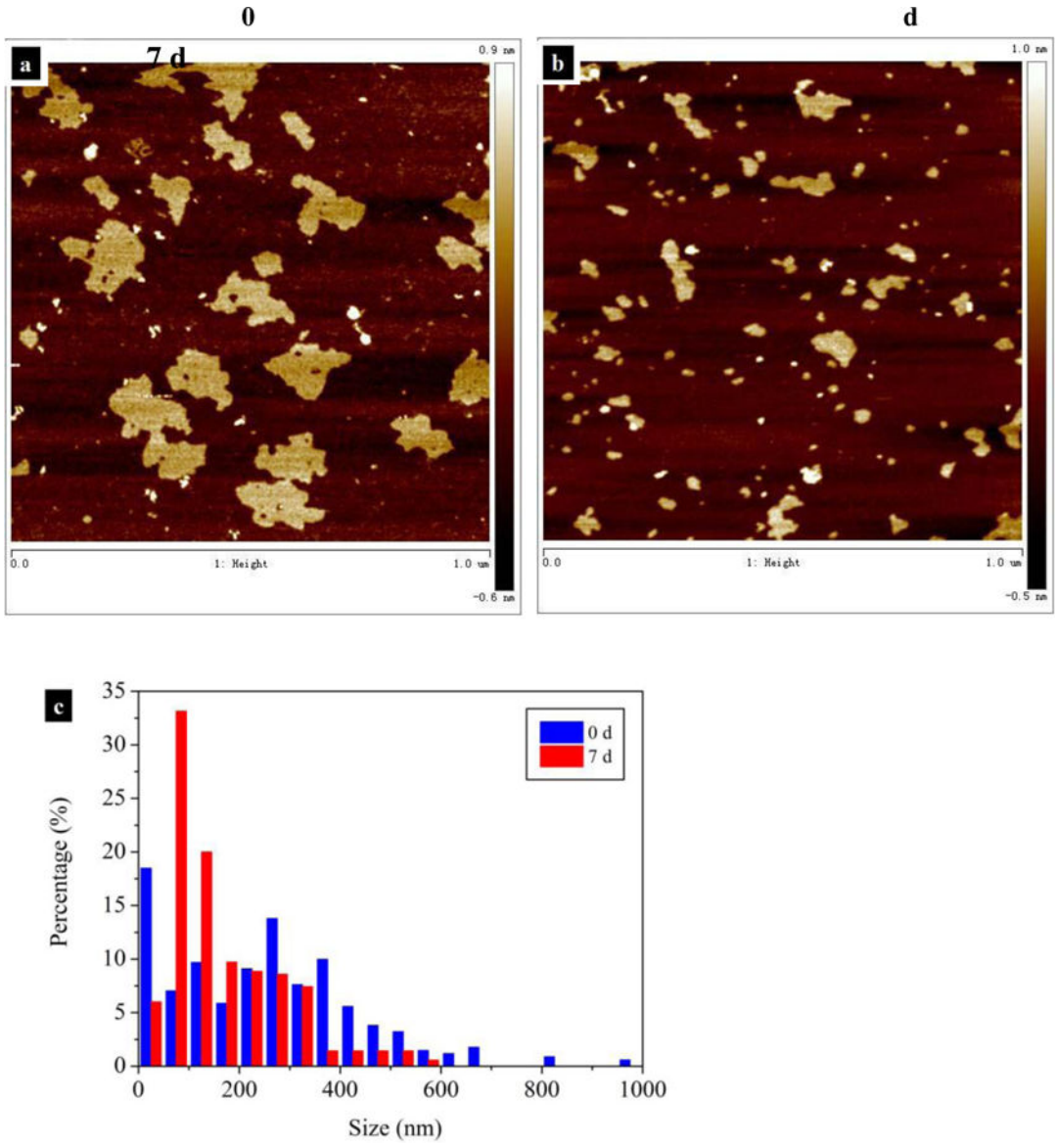

Fig. 4.

Morphological characterization of FLG that suspended in 10 mmol/L NaCl solution before and after sedimentation for one week. The concentrations of FLG were 1097 ± 20 and 823 ± 28) μg/L at 0 d and 7 d, respectively (n=3; uncertainties indicate standard deviation values). Representative AFM images of FLG sampled at 0 d (a) and 7 d (b). (c) Histogram of FLG size distribution. The histograms were developed by counting 300 sheets for each FLG sample.

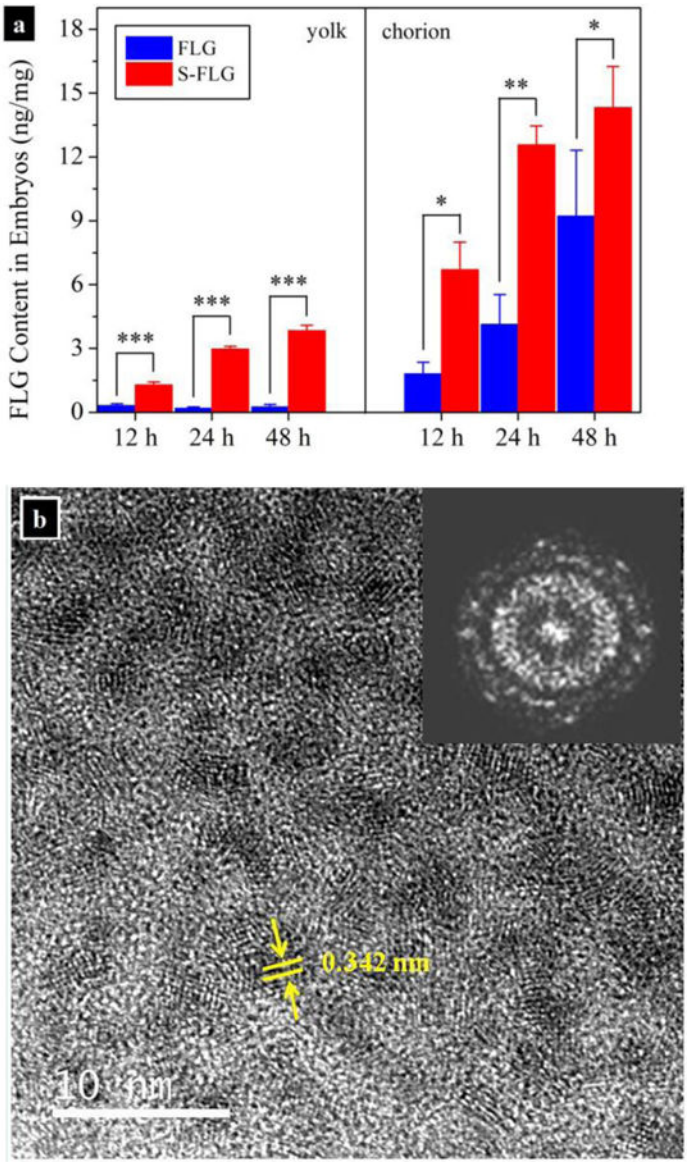

Fig. 5.

(a) Effects of lateral size on uptake of FLG by zebrafish embryos and distribution of FLG in chorion and yolk. *Z*ebrafish embryos were exposed to (75 ± 1) μg/L of FLG and small FLG (S-FLG) (n=3; uncertainties indicate standard deviation values). Data points are mean and standard deviation values that calculated from triplicate samples. Asterisks indicate statistical difference (*, $p<0.05$; **, $p<0.01$; ***, $p<0.001$) between treatments. (b) HRTEM images taken from ultra-thin section of the yolk that exposed to the S-FLG for 48 h; Inset: fourier transfer image of (b) indicates the crystalline structure of graphene.